Event-Triggered Multi-Model Predictive Control for Hypersonic Flight Vehicles

Zhengxiang Yang, Weiqiang Tang*, Peng Tian

School of Automation and Electrical Engineering, Lanzhou University of Technology, Lanzhou 730050, Gansu, China

*** Corresponding Author**

DOI: https://doi.org/10.51584/IJRIAS.2026.11070176

Received: 05 August 2026; Accepted: 10 August 2026; Published: 18 August 2026

ABSTRACT

The large-envelope velocity and altitude tracking of hypersonic flight vehicles is hindered by a combination of dynamic and practical constraints. Dynamically, it suffers from strong nonlinearities and varying operating points; practically, it contends with unavailable states, actuator limits, and the heavy computational burden imposed by periodic predictive optimization. This study proposes a tracking differentiator-based event-triggered state-feedback model predictive control (TD-ETSF-MPC) framework with multiple local prediction models. Three local linear models are built at representative equilibrium points and are activated based on the current operating condition. Meanwhile, a tracking differentiator provides smoothed reference commands, and a Luenberger observer estimates the unmeasured states for feedback. The proposed predictive controller directly accounts for actuator constraints within the finite-horizon framework. To reduce computational cost, online optimization is executed only when the estimated-state deviation from its value at the latest optimization instant exceeds a prescribed threshold or when the time since the last update reaches the maximum interval. Outside these conditions, the controller keeps the active model and the last computed control command. An event-triggered augmented error model is formulated to explicitly account for model switching, observer estimation errors, input holding, and bounded inter-update intervals. For the nominal closed-loop system, mode-dependent Lyapunov inequalities yield sufficient conditions for local exponential stability; this analysis is further extended to establish uniform ultimate boundedness in the presence of bounded disturbances. Simulation under simultaneous +30% parameter perturbations and high-frequency random disturbances shows that TD-ETSF-MPC achieves tracking performance comparable to TD-SF-MPC with satisfactory robustness. The update/hold indicator confirms that the optimization problem is solved only intermittently, thereby avoiding redundant online optimizations.

Keywords: event-triggered control; hypersonic flight vehicles; model predictive control; multi-model control; state observer.

INTRODUCTION

Hypersonic flight vehicles (HFVs) have considerable potential for rapid long-range transportation and time-critical aerospace missions because of their high speed, long range, rapid response, and maneuverability [1]. However, flight-control design remains challenging, particularly for air-breathing configurations, owing to strong aerodynamic–propulsive–structural coupling, nonlinear dynamics, parameter uncertainties, external disturbances, actuator constraints, and flexible modes [2]. Over the past two decades, HFV control has evolved from robust and nonlinear adaptive schemes [3, 4] toward predictive and multi-model methods capable of explicitly handling constraints and wide operating ranges.

Model predictive control (MPC) determines the current control action by solving a finite-horizon optimization problem and is well suited to constrained systems [5]. It has been applied to HFV velocity and altitude tracking under operational constraints [6]. Nevertheless, a model linearized at a single equilibrium point cannot accurately represent nonlinear dynamics over a large flight envelope. Multi-model predictive control (MMPC) addresses this limitation using a bank of local models and operating-condition-dependent controller switching [7]. Each local controller describes the vehicle near a representative operating point, improving prediction accuracy without requiring a fully nonlinear online prediction model. However, conventional MMPC solves an optimization problem at every sampling instant, resulting in unnecessary computational demand when the system remains close to its previously predicted trajectory.

Practical implementation is further complicated because not all feedback states are directly measurable. Output-feedback control [8] and state-estimator-integrated control under noisy measurements [9] have therefore been investigated for HFVs. Although state estimation can provide the information required by predictive controllers and mitigate the effects of measurement noise, it does not eliminate the repeated optimization inherent in tracking-differentiator-based state-feedback model predictive control (TD-SF-MPC) or the associated frequent control updates.

Event-triggered control updates the controller only when a prescribed condition is satisfied, thereby avoiding redundant periodic executions [10, 11]. In event-triggered MPC, a new optimal sequence is computed only when an event is triggered; otherwise, the previous control action is retained. It has been developed for constrained nonlinear systems with bounded disturbances [12], while event-triggered intermittent sampling has been introduced for nonlinear MPC [13]. Dynamic event-triggered robust MPC has also been applied to attitude tracking of air-breathing HFVs with disturbance preview [14]. Nevertheless, existing studies mainly focus on single-model systems or attitude subsystems. Event-triggered MMPC for large-envelope flexible HFVs remains insufficiently investigated, particularly when model switching, unavailable states, input holding, and closed-loop stability must be addressed simultaneously.

To fill this gap, this paper develops a tracking-differentiator-based event-triggered state-feedback model predictive control (TD-ETSF-MPC) method for large-envelope velocity and altitude tracking of a flexible HFV. Simulation under composite uncertainties combining +30% parameter perturbations and high-frequency random disturbances demonstrates accurate tracking and satisfactory robustness. Compared with TD-SF-MPC, the proposed TD-ETSF-MPC method maintains comparable tracking performance while avoiding optimization at non-triggering instants. The main contributions are summarized as follows:

1) A TD-ETSF-MPC architecture is developed using three local linear prediction models and an operating-condition-dependent switching rule. The method combines the large-envelope adaptability of multiple-model control with the constraint-handling capability of MPC and event-based optimization updates.

2) An observer-based triggering mechanism is designed for partially unavailable states. A Luenberger observer reconstructs the states required by the feedback law, while the estimated-state deviation from the latest triggering instant determines whether the optimization is updated or the previous control action is retained.

3) A unified stability analysis is established for the switched event-triggered closed-loop system. Sufficient conditions for nominal local exponential stability are derived by jointly considering model switching, observer errors, input holding, and bounded inter-update intervals; the analysis is further extended to uniform ultimate

boundedness under bounded disturbances.

The remainder of this paper is organized as follows. Section 2 presents the flexible HFV model. Section 3 develops the proposed controller. Section 4 provides the stability analysis. Section 5 presents the simulations, and Section 6 concludes the paper.

PROBLEM FORMULATION

Nonlinear Longitudinal Dynamics

The longitudinal model of a hypersonic flight vehicle is adopted from [6] and is given in (1). Under the symmetric-flight assumption, the lateral variables are neglected, and the coupled rigid-body and flexible dynamics are expressed as:

$$\begin{cases} \dot{V} = \dfrac{T\cos\alpha - D}{m} - g\sin\gamma + d_1, \\ \dot{\gamma} = \dfrac{L + T\sin\alpha}{mV} - \dfrac{g\cos\gamma}{V} + d_2, \\ \dot{h} = V\sin\gamma + d_3, \\ \dot{\alpha} = q - \dot{\gamma} + d_4, \\ \dot{q} = \dfrac{M}{I_{yy}} + d_5, \\ \ddot{\eta}_i = -2\xi_i\omega_i\dot{\eta}_i - \omega_i^2\eta_i + N_i \quad i = 1,2,3, \end{cases} \tag{1}$$

where V, γ, h, α, and q denote the velocity, flight-path angle, altitude, angle of attack, and pitch rate, respectively. The variables η_i, ξ_i, and ω_i represent the i-th flexible-mode displacement, damping ratio, and natural frequency. The modal damping ratios are $\xi_i = 0.02$, and the first three natural frequencies are 21.17, 53.29, and 109.1 rad/s, respectively. Moreover, m, g, and I_{yy} are the vehicle mass, gravitational acceleration, and pitch moment of inertia, while d_i denotes the external disturbance acting on the corresponding rigid-body state.

The state, control-input, and controlled-output vectors are defined as:

$$\begin{cases} \mathbf{x} = [V, \gamma, h, \alpha, q, \eta_1, \dot{\eta}_1, \eta_2, \dot{\eta}_2, \eta_3, \dot{\eta}_3]^{\mathrm{T}}, \\ \mathbf{u} = [\Phi, \delta_e]^{\mathrm{T}}, \mathbf{y} = [V, h]^{\mathrm{T}}, \end{cases} \tag{2}$$

where Φ is the fuel-equivalence ratio and δ_e is the elevator deflection. The canard and elevator deflections satisfy $\delta_c = k_{ec}\delta_e$ and $k_{ec} = -\dfrac{C_L^{\delta_e}}{C_L^{\delta_c}}$. The thrust, aerodynamic forces, pitching moment, and generalized flexible forces are described by:

$$\begin{cases} T = \bar{q}S\left[C_{T,\Phi}(\alpha)\Phi + C_T(\alpha) + C_T^{\eta}\boldsymbol{\eta}\right] \\ L = \bar{q}SC_L(\alpha,\boldsymbol{\delta},\boldsymbol{\eta}) \\ D = \bar{q}SC_D(\alpha,\boldsymbol{\delta},\boldsymbol{\eta}) \\ M = z_T T + \bar{q}S\bar{c}, C_M(\alpha,\boldsymbol{\delta},\boldsymbol{\eta}) \\ N_i = \bar{q}S\left[N_i^{\alpha^2}\alpha^2 + N_i^{\alpha}\alpha + N_i^{\delta_e}\delta_e + N_i^{\delta_c}\delta_c + N_i^0 + N_i^{\eta}\boldsymbol{\eta}\right] \end{cases} \tag{3}$$

where $\bar{q}=\frac{1}{2}\rho V^2$ is the dynamic pressure, ρ is the atmospheric density, S is the reference area, $\bar{c}$ is the mean aerodynamic chord, z_T is the thrust moment arm, $\boldsymbol{\delta}=[\delta_c,\delta_e]^{\mathrm{T}}$ and $\boldsymbol{\eta}$ collects the three flexible modes and their derivatives. Equations (1-3) constitute the nonlinear plant used in the subsequent simulations. More details about the model can be found in [6].

Local Linear Prediction Models

A single model linearized at one equilibrium point cannot accurately describe the vehicle dynamics throughout the considered flight envelope. The nonlinear model is first written in the compact form:

$$\dot{\mathbf{x}} = \mathbf{f}(\mathbf{x},\mathbf{u},\mathbf{d}), \qquad \mathbf{y} = \mathbf{g}(\mathbf{x}) \tag{4}$$

where $\mathbf{d}$ collects the external disturbances. For the i-th equilibrium point $(\mathbf{x}_i^*,\mathbf{u}_i^*)$, satisfying $\mathbf{f}(\mathbf{x}_i^*,\mathbf{u}_i^*,\mathbf{0})=\mathbf{0}$, the Jacobian matrices are defined as:

$$\begin{cases} A_i = \left.\dfrac{\partial \mathbf{f}}{\partial \mathbf{x}}\right|_{(\mathbf{x}_i^*,\mathbf{u}i^*)}, \\ B_i = \left.\dfrac{\partial \mathbf{f}}{\partial \mathbf{u}}\right|(\mathbf{x}_i^*,\mathbf{u}i^*), \\ C_i = \left.\dfrac{\partial \mathbf{g}}{\partial \mathbf{x}}\right|\mathbf{x}_i^*. \end{cases} \tag{5}$$

Defining $\Delta\mathbf{x} = \mathbf{x}-\mathbf{x}_i^*$, $\Delta\mathbf{u} = \mathbf{u}-\mathbf{u}_i^*$, and $\Delta\mathbf{y} = \mathbf{y}-\mathbf{y}_i^*$, the local linear model is obtained as:

$$\begin{cases} \Delta\dot{\mathbf{x}} = A_i\Delta\mathbf{x} + B_i\Delta\mathbf{u}, \\ \Delta\mathbf{y} = C_i\Delta\mathbf{x}, \qquad i \in \mathrm{I} \ = \{1,2,3\}. \end{cases} \tag{6}$$

Three representative operating points are selected along the large-envelope maneuver:

$$\begin{cases} V_1^* = 7846.4 \text{ ft/s}, \quad h_1^* = 85000 \text{ ft}, \\ V_2^* = 8046.4 \text{ ft/s}, \quad h_2^* = 85300 \text{ ft}, \\ V_3^* = 8246.4 \text{ ft/s}, \quad h_3^* = 85600 \text{ ft}. \end{cases} \tag{7}$$

Under zero-order-hold discretization with sampling period T_s, each continuous-time local model is discretized as:

INTERNATIONAL JOURNAL OF RESEARCH AND INNOVATION IN APPLIED SCIENCE (IJRIAS)
ISSN No. 2454-6194 | DOI: 10.51584/IJRIAS |Volume XI Issue VII July 2026

$$\begin{cases} \Delta \mathbf{x}_{k+1} = A_{d,i}\Delta \mathbf{x}_k + B_{d,i}\Delta \mathbf{u}_k, \\ \Delta \mathbf{y}_k = C_{d,i}\Delta \mathbf{x}_k, \\ A_{d,i} = e^{A_i T_s}, \\ B_{d,i} = \int_0^{T_s} e^{A_i \tau} B_i, d\tau, \\ C_{d,i} = C_i. \end{cases} \tag{8}$$

For notational simplicity, the subscript d and the incremental symbol Δ are omitted in the subsequent controller design. The active model index is determined by the switching rule introduced in Section 3.

Control Objectives and Constraints

The primary control objective is to make the vehicle velocity and altitude track their reference commands. Let $\mathbf{r}_k = [V_{r,k}, h_{r,k}]^{\mathrm{T}}$ denote the reference vector. The tracking error and the nominal convergence objective are defined as:

$$\mathbf{e}_k = \mathbf{y}_k - \mathbf{r}_k, \qquad \lim_{k\to\infty} \|\mathbf{e}_k\| = 0, \tag{9}$$

where $\mathbf{d} = \mathbf{0}$.

Meanwhile, all remaining rigid-body and flexible states should remain bounded in the presence of parameter perturbations and external disturbances. The physical limitations of the fuel-equivalence ratio and elevator deflection are imposed as:

$$0.05 \le \Phi_k \le 2, \qquad -20^\circ \le \delta_{e,k} \le 20^\circ. \tag{10}$$

Because some states required by the feedback controller are not directly available, a state observer is introduced to reconstruct the unavailable information. Based on the local prediction models, the controller developed in Section 3 is required to satisfy the input constraints, accommodate changes in operating conditions, and reduce unnecessary online optimization updates through an event-triggering mechanism.

Event-Triggered Multi-Model Predictive Control Design

Observer-Based State Reconstruction

To account for variations in vehicle dynamics over the considered flight envelope, a hard-switching mechanism is employed to select the local model that best matches the current operating condition. Specifically, the active model is determined from the distance between the current output and the three equilibrium outputs:

$$i_k = \arg\min_{i\in \mathrm{I}} \left\| W_s\left(\mathbf{y}_k - \mathbf{y}_i^*\right)\right\|_2, \qquad W_S = \mathrm{diag}(w_V, w_h), \tag{11}$$

where $\mathrm{I} = \{1,2,3\}$, $\mathbf{y}_i^* = [V_i^*, h_i^*]^{\mathrm{T}}$, and W_S is a positive diagonal scaling matrix used to compensate for the different numerical ranges of velocity and altitude. If the minimum distance is attained by multiple models, the previously active model is retained to avoid unnecessary switching.

Some rigid-body and flexible states required by the predictive controller may not be directly available. Let $\mathbf{y}_{m,k} = C_{m,i_k}\mathbf{x}_k$ denote the available measurement vector. Based on the active local model, a discrete-time Luenberger observer is constructed as:

$$\hat{\mathbf{x}}_{k+1} = A_{i_k}\hat{\mathbf{x}}_k + B_{i_k}\mathbf{u}_k + L_{i_k}(\mathbf{y}_{m,k} - C_{m,i_k}\hat{\mathbf{x}}_k), \tag{12}$$

where $\hat{\mathbf{x}}_k$ is the estimated state and L_{i_k} is the observer gain. Defining the estimation error as: $\tilde{\mathbf{x}}_k = \mathbf{x}_k - \hat{\mathbf{x}}_k$, its dynamics are given by:

$$\tilde{\mathbf{x}}_{k+1} = \left(A_{i_k} - L_{i_k}C_{m,i_k}\right)\tilde{\mathbf{x}}_k, \quad \mathbf{x}_k^f = \mathbf{x}_k - (I - M)\tilde{\mathbf{x}}_k. \tag{13}$$

where M is a diagonal measurement-selection matrix. An entry equal to one indicates that the corresponding state is directly available, whereas an entry equal to zero indicates that its observer estimate is used. Thus, $\mathbf{x}_k^f$ combines the measured and estimated states and is used as the feedback vector of the MMPC controller. The gains L_i are selected such that $A_i - L_iC_{m,i}$ is Schur stable. The convergence of the observer error under model switching is analyzed in Section 4.

Constrained Multi-Model Predictive Control

Abrupt changes in the velocity and altitude commands may produce large initial tracking errors and aggressive actuator responses. Therefore, the reference commands are processed by a tracking differentiator before being supplied to the predictive controller [15]:

$$\begin{cases} v_{1,k+1} = v_{1,k} + T_s v_{2,k}, \\ v_{2,k+1} = v_{2,k} + T_s f_{\text{han}}\left(v_{1,k} - v_{0,k}, v_{2,k}, r_{\text{td}}, h_{\text{td}}\right). \end{cases} \tag{14}$$

where $v_{0,k}$ is the original command, $v_{1,k}$ is the smoothed reference, $v_{2,k}$ is its derivative, r_{td} and h_{td} are the tracking and integration parameters, respectively. Equation (14) is independently applied to the velocity and altitude commands. The resulting signals are used to construct the reference state $\mathbf{x}_{r,k}$, while the reference values of the remaining incremental states are set to zero.

To obtain a stable transformed output for predictive control, a nonsingular matrix T_i is selected for each local model such that:

$$\begin{cases} T_iB_i = \begin{bmatrix} 0_{(n-m)\times m} \\ B_{2,i} \end{bmatrix}, \\ T_iA_iT_i^{-1} = \begin{bmatrix} A_{11,i} & A_{12,i} \\ A_{21,i} & A_{22,i} \end{bmatrix}, \\ \chi_i = \begin{bmatrix} K_i & I_m \end{bmatrix} T_i, \end{cases} \tag{15}$$

ISSN No. 2454-6194 | DOI: 10.51584/IJRIAS |Volume XI Issue VII July 2026

where $B_{2,i} \in \mathbb{R}^{m\times m}$ is nonsingular. The gain K_i is chosen such that $A_{11,i} - A_{12,i}K_i$ is Schur stable. The transformed feedback and reference outputs are consequently defined as $\boldsymbol{\sigma}_k = \chi_i \mathbf{x}_k^f$ and $\boldsymbol{\sigma}_{r,k} = \chi_i \mathbf{x}_{r,k}$.

Let N_p and N_u denote the prediction and control horizons, respectively, with $N_u \le N_p$. The predicted transformed output over the prediction horizon can be written in the compact form:

$$\begin{cases} \boldsymbol{\Sigma}_k = \mathrm{F}_i \mathbf{x}_k^f + \mathrm{G}_i \mathbf{U}_k, \\ \boldsymbol{\Sigma}_{r,k} = \mathrm{col}\left(\boldsymbol{\sigma}_{r,k+1}, \ldots, \boldsymbol{\sigma}_{r,k+N_p}\right), \\ \mathbf{U}_k = \mathrm{col}\left(\mathbf{u}_{k|k}, \ldots, \mathbf{u}_{k+N_u-1|k}\right), \end{cases} \tag{16}$$

where F_i and G_i are the lifted prediction matrices constructed from A_i, B_i, and χ_i. After the control horizon, the final predicted control input is held constant.

The finite-horizon performance index is selected as:

$$J_k = \left\|\boldsymbol{\Sigma}_k - \boldsymbol{\Sigma}_{r,k}\right\|_{\bar{Q}}^2 + \left\|\mathbf{U}_k\right\|_{\bar{R}}^2 \tag{17}$$

where $\bar{Q} \pm 0$ and $\bar{R} \succ 0$ are block-diagonal weighting matrices. Substituting (16) into (17) yields the constrained quadratic programming problem:

$$\begin{cases} \mathbf{U}_k^* = \arg\min\limits_{\mathbf{U}_k} \dfrac{1}{2} \mathbf{U}_k^{\mathrm{T}} H_i \mathbf{U}_k + \mathbf{f}_{i,k}^{\mathrm{T}} \mathbf{U}_k, \\ G_{c,i} \mathbf{U}_k \le \mathbf{b}_{c,i}, \end{cases} \tag{18}$$

where $H_i = 2\left(\mathrm{G}_i^{\mathrm{T}} \bar{Q} \mathrm{G}_i + \bar{R}\right)$ and $\mathbf{f}_{i,k} = 2\mathrm{G}_i^{\mathrm{T}} \bar{Q}\left(\mathrm{F}_i \mathbf{x}_k^f - \boldsymbol{\Sigma}_{r,k}\right)$. Because $\bar{R} \succ 0$, the Hessian matrix H_i is positive definite and the optimization problem has a unique solution whenever the constraint set is feasible.

The constraint matrices in (18) incorporate both the actuator-amplitude and actuator-rate limitations:

$$\underline{\mathbf{u}} \le \mathbf{u}_{k+\ell|k} \le \bar{\mathbf{u}}, \qquad \underline{\Delta \mathbf{u}} \le \mathbf{u}_{k+\ell|k} - \mathbf{u}_{k+\ell-1|k} \le \overline{\Delta \mathbf{u}}, \qquad \ell = 0, \ldots, N_u - 1. \tag{19}$$

where $\underline{\mathbf{u}} = \begin{bmatrix} 0.05 & -20^\circ \end{bmatrix}^{\mathrm{T}}$ and $\bar{\mathbf{u}} = \begin{bmatrix} 2 & 20^\circ \end{bmatrix}^{\mathrm{T}}$. When the prediction model is expressed in local incremental coordinates, the physical input bounds are shifted by the equilibrium input $\mathbf{u}_i^*$ before constructing $\mathbf{b}_{c,i}$. For $\ell = 0$, the term $\mathbf{u}_{k-1|k}$ denotes the previously applied control input expressed in the current local coordinates.

ISSN No. 2454-6194 | DOI: 10.51584/IJRIAS |Volume XI Issue VII July 2026

Event-Triggered Optimization Mechanism

Conventional MMPC solves (18) at every sampling instant. To reduce redundant online optimization, the proposed method updates the optimal control sequence only when the estimated state variation exceeds a prescribed threshold or the maximum allowable inter-update interval is reached.

Let k_j denote the most recent optimization instant and let i_{k_j} denote the local model selected at that instant.

The selected prediction model is retained over the interval $\left[k_j, k_{j+1}\right)$ and is updated at the next optimization instant. Consistent with the original implementation, the triggering variable is constructed from the estimated rigid-body states:

$$\begin{cases} \hat{\mathbf{z}}_k = S_t \mathbf{x}_k, \\ \mathbf{e}_k = \hat{\mathbf{z}}_k - \hat{\mathbf{z}}_{k_j}, \\ S_t = \left[I_5 \quad 0_{5\times 6} \right]. \end{cases} \tag{20}$$

All states in (20) are expressed in local incremental coordinates so that the equilibrium offsets do not enter the triggering condition. The next optimization instant is defined as:

$$k_{j+1} = \min\left\{ k_j + N_{\max}, \inf\left\{ k \ge k_j + N_d : \left\|\mathbf{e}_k\right\|_2 \ge \iota \left\|\hat{\mathbf{z}}_{k_j}\right\|_2 \right\} \right\} \tag{21}$$

where $\iota > 0$ is the triggering threshold, $N_d \ge 1$ is the minimum inter-event interval, and $N_{\max} > N_d$ is the maximum allowable inter-event interval. The inner condition generates a state-dependent update, whereas the first term enforces a timeout update when the state-dependent condition remains unsatisfied. If the set in the infimum is empty, its infimum is taken as $+\infty$. Therefore, the resulting inter-event interval $h_j = k_j + 1 - k_j$ satisfies $N_d \le h_j \le N_{\max}$. The minimum interval prevents excessively frequent optimization updates, while the maximum interval guarantees that the control sequence is recomputed within a finite number of sampling periods.

At $k_0 = 0$, the optimization problem is solved unconditionally. At each subsequent update instant, generated either by the state-dependent condition or by the timeout condition, the active model is selected using (11), and a new optimal control sequence is calculated from (18). The selected model and the resulting control command are retained until the next update instant:

$$\mathbf{u}_k^{\text{act}} = \begin{cases} \mathbf{u}_{i_{k_j}}^* + E_1 \mathbf{U}_{k_j}^*, & k = k_j, \\ \mathbf{u}_{k_j}^{\text{act}}, & k_j < k < k_{j+1}, \end{cases} \tag{22}$$

where $E_1 = \left[I_2 \quad 0 \quad \cdots \quad 0 \right]$. At non-triggering instants, the controller only updates the state observer and evaluates the triggering condition; the quadratic programming problem is not resolved. These operations avoid solving the quadratic programming problem at non-triggering instants. Moreover, the held command remains within the actuator-amplitude constraints because it was feasible at the latest optimization instant, while its variation is zero throughout the input-hold interval. The bounded inter-event interval established in (21) will be used to construct the event-to-event augmented closed-loop model and derive the stability conditions in Section 4.

Stability Analysis

Event-to-Event Augmented Error Model

The stability analysis is conducted in a neighborhood of the tracking equilibrium. The smoothed reference generated by the tracking differentiator is assumed to have converged to a constant value. Moreover, the input constraints are assumed to be inactive in this neighborhood, so that the quadratic programming problem in (18) admits its unconstrained solution. Accordingly, the result established below concerns the local stability of the nominal closed-loop system.

Define the tracking error as $\mathbf{z}_k = \mathbf{x}_k - \mathbf{x}_r$. All local prediction models are expressed in this common tracking-error coordinate. At an optimization instant k_j, the first element of the unconstrained optimal control sequence can be written as

$$\begin{cases} \Delta \mathbf{u}_{k_j} = \mathrm{K}_i \mathbf{z}_{k_j}^f \\ \qquad = \mathrm{K}_i \left(\mathbf{z}_{k_j} - \Pi \tilde{\mathbf{x}}_{k_j} \right), \\ \Pi = I - M, \\ \mathrm{K}_i n = -E_1 \left(\mathrm{G}_i^{\mathrm{T}} \bar{Q} \mathrm{G}_i + \bar{R} \right)^{-1} \mathrm{G}_i^{\mathrm{T}} \bar{Q} \mathrm{F}_i, \end{cases} \tag{23}$$

where $i = i_{k_j}$ is the local model selected at k_j, and K_i is the first-move MMPC feedback gain. Let $h_j = k_{j+1} - k_j$ denote the inter-event interval. According to (21), the admissible inter-event intervals form the finite set $h_j \in \mathrm{H} \equiv \{N_d, N_d + 1, \ldots, N_{\max}\}$. The minimum and maximum inter-update intervals are set to $N_d = 2$ and $N_{\max} = 20$, yielding $\mathrm{H} = \{2, 3, \ldots, 20\}$. The selected model and the control command in (23) are retained over $\left[k_j, k_{j+1}\right)$. Define $\Gamma_{i,h} \sum_{r=0}^{h-1} A_i^r B_i$, thus iterating the local prediction model for h_j sampling periods gives:

$$\mathbf{z}_{k_{j+1}} \left(A_i^{h_j} + \Gamma_{i,h_j} \mathrm{K} i \right) \mathbf{z}_{k_j} \Gamma_{i,h_j} \mathrm{K}_i \Pi \tilde{\mathbf{x}} k_j. \tag{24}$$

Meanwhile, it follows from (13) that the observer error at two consecutive optimization instants satisfies $\tilde{\mathbf{x}}_{k_{j+1}} = A_{o,i}^{h_j} \tilde{\mathbf{x}}_{k_j}$ and $A_{o,i} = A_i - L_i C_{m,i}$. Define the augmented error at the optimization instants as $\xi_j = \begin{bmatrix} \mathbf{z}_{k_j} \\ \tilde{\mathbf{x}}_{k_j} \end{bmatrix}$.

Equations (24) and (13) can then be combined into the event-to-event augmented system:

$$\begin{cases} \xi_{j+1} = \mathrm{A} i, h_j \xi j, \\ \mathrm{A}_{i,h} = \begin{bmatrix} A_i^h + \Gamma_{i,h} \mathrm{K}_i & -\Gamma_{i,h} \mathrm{K}_i \Pi \\ 0 & A_{o,i}^h \end{bmatrix}. \end{cases} \tag{25}$$

ISSN No. 2454-6194 | DOI: 10.51584/IJRIAS |Volume XI Issue VII July 2026

Unlike a one-step closed-loop representation, (25) explicitly includes the input-hold operation, the observer error, the inter-event interval, and the active local model.

Main Stability Result

Let $\mathcal{S} \subseteq \mathcal{I} \times \mathcal{I}$ denote the set of allowable transitions between the local models. The following theorem establishes a sufficient condition for the stability of the nominal TD-ETSF-MPC system.

Theorem 1. Consider the augmented event-to-event system (25). Suppose that the reference is constant, the optimization problem remains feasible with inactive constraints in a neighborhood $\mathcal{X}_0$ of the equilibrium, and the event interval satisfies $h_j \in \mathcal{H}$. If there exist symmetric matrices $P_i \succ 0$ and $Q_{i\ell h} \succ 0$ such that

$$\mathrm{A}_{i,h}^{\mathrm{T}} P_\ell \mathrm{A}_{i,h} - P_i \prec -Q_{i\ell h}, \tag{26}$$

for every $(i,\ell) \in \mathcal{S}$ and every $h \in \mathcal{H}$, then the origin of the nominal augmented error system is locally exponentially stable.

Proof. Consider the mode-dependent Lyapunov function $V_j = \xi_j^{\mathrm{T}} P_{i_j} \xi_j$. Suppose that the active model changes from $i = i_j$ to $\ell = i_{j+1}$ at the next optimization instant. Using (25), the Lyapunov difference satisfies:

$$\begin{aligned} V_{j+1} - V_j &= \xi_j^{\mathrm{T}} \left(\mathrm{A}_{i,h_j}^{\mathrm{T}} P_\ell \mathrm{A}_{i,h_j} - P_i \right) \xi_j \\ &\le -\xi_j^{\mathrm{T}} Q_{i\ell h_j} \xi_j \\ &\le -\lambda_{\min}\left(Q_{i\ell h_j} \right) \left\| \xi_j \right\|_2^2 . \end{aligned} \tag{27}$$

Since $\mathcal{I}$, $\mathcal{S}$, and $\mathcal{H}$ are finite sets, the smallest eigenvalue of $Q_{i\ell h}$ admits a uniform positive lower bound. Similarly, the eigenvalues of P_i admit uniform positive lower and upper bounds. Consequently, V_j decreases exponentially at the optimization instants, which implies $\lim_{j\to\infty} \xi_j = 0$. For every $k = k_j + r$, where $0 \le r < h_j \le N_{\max}$, the state is obtained by applying a finite number of bounded state-transition matrices to ξ_j. Therefore, convergence at the optimization instants also guarantees convergence at all intermediate sampling instants. It follows that $\lim_{k\to\infty} \mathbf{z}_k = 0$ and $\lim_{k\to\infty} \tilde{\mathbf{x}} = 0$.

Hence, the nominal TD-ETSF-MPC closed-loop system is locally exponentially stable. In addition, condition (26) forms a finite set of linear matrix inequalities once the controller and observer gains are fixed. It simultaneously accounts for the three local models, all admissible model transitions, and all possible inter-event intervals. A common quadratic Lyapunov function is obtained as the special case $P_1 = P_2 = P_3$.

Extension to Nonlinear Dynamics and Bounded Disturbances

The local prediction models neglect the higher-order terms generated by linearizing the nonlinear HFV dynamics. Incorporating these terms and a bounded disturbance into (25) gives:

$$\boldsymbol{\xi}_{j+1} = \mathrm{A}_{i,h_j}\boldsymbol{\xi}_j + \boldsymbol{\varphi}_{i,h_j}\left(\boldsymbol{\xi}_j\right) + \mathrm{W}_{i,h_j}\mathbf{d}_j, \tag{28}$$

where $\boldsymbol{\varphi}_{i,h_j}$ denotes the accumulated linearization remainder. In a sufficiently small neighborhood of the equilibrium, the smooth nonlinear model satisfies $\left\|\boldsymbol{\varphi}_{i,h}(\boldsymbol{\xi})\right\|_2^2 \le c_i \left\|\boldsymbol{\xi}\right\|_2^2$. The quadratic remainder can therefore be dominated by the strict Lyapunov decrease provided by (26). For the disturbed system, standard quadratic bounds yield:

$$V_{j+1} - V_j \le -\alpha\left\|\boldsymbol{\xi}_j\right\|_2^2 + \beta\left\|\mathbf{d}_j\right\|_2^2, \tag{29}$$

where $\alpha > 0$ and $\beta > 0$ are constants. Consequently, the nonlinear nominal closed-loop system is locally asymptotically stable when $\mathbf{d}_j = 0$. If $\left\|\mathbf{d}_j\right\|_2 \le \bar{d}$, the augmented tracking error is uniformly ultimately bounded and satisfies

$$\limsup_{j\to\infty}\left\|\boldsymbol{\xi}_j\right\|_2 \le c_d\bar{d}, \tag{30}$$

where $c_d > 0$ is a constant. Thus, persistent disturbances do not generally permit exact asymptotic tracking, but the tracking and observer errors remain bounded within a disturbance-dependent neighborhood of the equilibrium.

Simulation Results

The initial velocity and altitude are 7846.4ft/s and 85000ft, respectively. The command increments are $\Delta V = 600\text{ft/s}$ and $\Delta h = 900\text{ft}$. The corresponding parameters are $T_s = 0.01\text{s}$, $\iota = 0.6$ and $p = 0.495$. TD-SF-MPC is adopted as the baseline and solves the quadratic programming problem at every sampling instant using the full plant state. TD-ETSF-MPC uses the same local model bank, prediction parameters, constraints, and reference commands, but reconstructs unavailable states through the observer and updates the optimal command according to (21). The parameters of the three local predictive controllers are listed in **Table 1**. The operating conditions are considered as follows: $\bar{c}$, ρ, m, I_{yy}, g, and z_T are simultaneously increased by 30%, the five rigid-body state variables in (1) are subject to external disturbances:

$$\mathbf{d}_k = \begin{bmatrix}0.005 & 0.001 & 0.008 & 0.004 & 0.003\end{bmatrix}^{\mathrm{T}} f_{\text{noise},k}, \tag{31}$$

where $f_{\text{noise},k}$ is a high-pass-filtered random signal generated from uniformly distributed noise in the interval $[-0.6, 0.6]$. The response of the system under composite uncertainties is shown in Fig. 1.

ISSN No. 2454-6194 | DOI: 10.51584/IJRIAS |Volume XI Issue VII July 2026

Table 1. Parameters of the local predictive controllers

Parameter	**Controller 1**	**Controller 2**	**Controller 3**
Prediction horizon N_P	83	86	90
Control horizon N_u	40	35	45
Velocity tracking factor	7.5	7.5	7.5
Altitude tracking factor	18	18	18
Velocity-error weight	800	1000	900
Altitude-error weight	2000	2000	4000
Control-increment weight r_1	500	500	500
Control-increment weight r_2	400	400	400

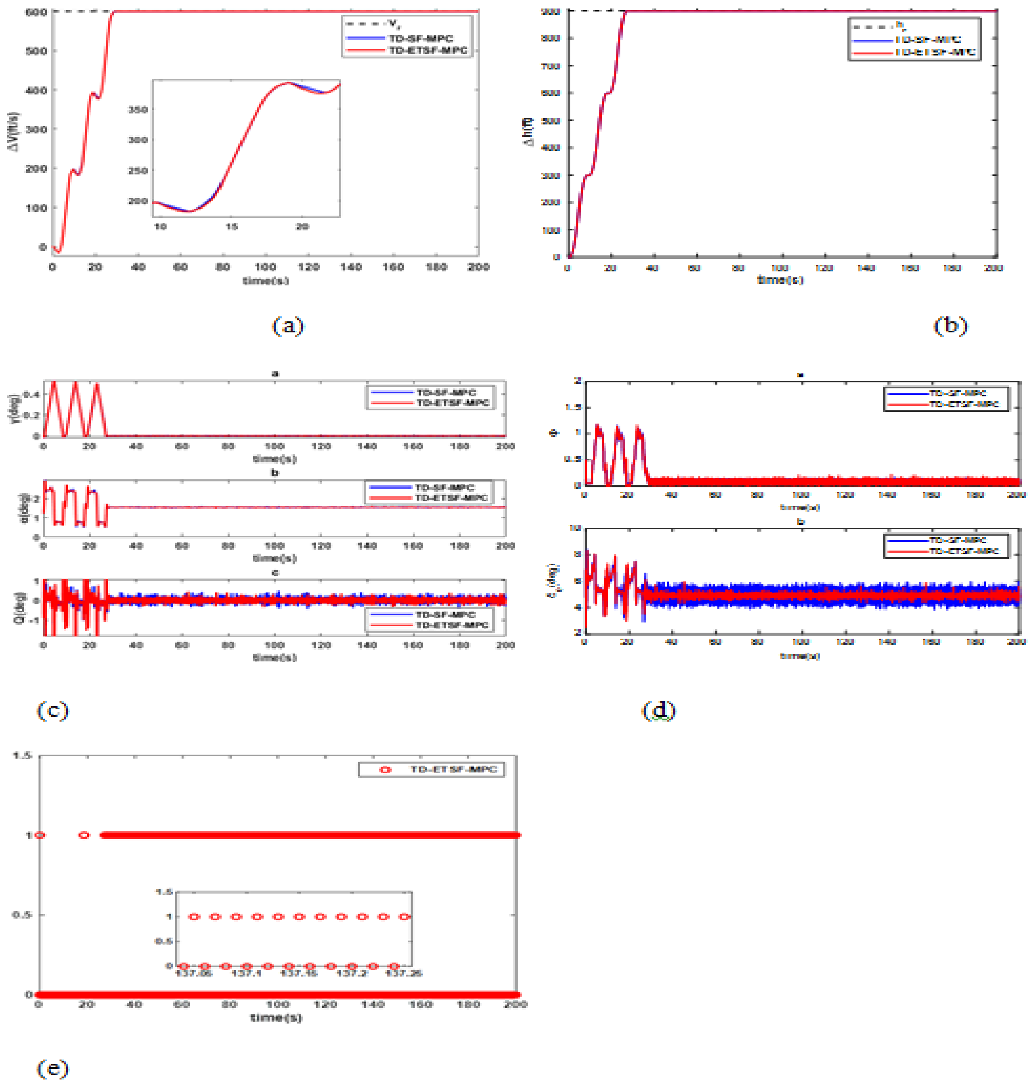

Fig. 1. System response. (a) Velocity, (b) Altitude, (c) Other variables, (d) Control input, (e) Event-triggered situations.

As shown in Fig. 1(a), the two controllers provide nearly identical velocity-increment tracking. Small transient deviations occur at model-switching instants because of mismatch between adjacent local prediction models. The corresponding effect is less pronounced in the altitude-increment response in Fig. 1(b). Figure 1(c) shows that the internal states remain bounded under the composite uncertainties, although high-frequency disturbances induce oscillations, most visibly in the pitch rate. The control inputs in Fig. 1(d) also remain bounded. TD-ETSF-MPC exhibits slightly smaller high-frequency input oscillations than TD-SF-MPC; this result reflects the overall closed-loop architecture, including observer-based feedback and input holding, and should not be attributed solely to the triggering rule. Fig. 1(e) presents the optimization-update/input-hold indicator, where 0 denotes a new online optimization and 1 denotes retention of the previously computed control command. The occurrence of both update and hold instants confirms that the quadratic programming problem is not solved at every sampling instant. Thus, TD-ETSF-MPC maintains tracking performance comparable to TD-SF-MPC under the composite uncertainties while avoiding redundant online optimizations.

CONCLUSION

An observer-based TD-ETSF-MPC framework was developed for large-envelope velocity and altitude tracking of a flexible HFV. Three local prediction models, a Luenberger observer, and an event-triggering mechanism were integrated to address operating-point variations, unavailable states, actuator constraints, and redundant online optimization. The event-to-event Lyapunov analysis established sufficient conditions for nominal local exponential stability and uniform ultimate boundedness under bounded disturbances. Under simultaneous +30% parameter perturbations and high-frequency random disturbances, TD-ETSF-MPC achieved tracking performance comparable to TD-SF-MPC, while the update indicator confirmed that the quadratic programming problem was not solved at every sampling instant. Future work will address adaptive triggering thresholds and hardware-in-the-loop validation.

Funding: This work was supported by the National Natural Science Foundation of China (grant number 62463017).

REFERENCES

1. W. Tang, Z. Yang, C. Jia and H. Gao, “Fixed-time sliding mode controller design for hypersonic vehicles,” Aircraft Engineering and Aerospace Technology, vol. 98, no. 3, pp. 487–501, 2026.
2. M. A. Bolender and D. B. Doman, “Nonlinear longitudinal dynamical model of an air-breathing hypersonic vehicle,” Journal of Spacecraft and Rockets, vol. 44, no. 2, pp. 374–387, 2007.
3. L. Fiorentini, A. Serrani, M. A. Bolender, and D. B. Doman, “Nonlinear robust adaptive control of flexible air-breathing hypersonic vehicles,” Journal of Guidance, Control, and Dynamics, vol. 32, no. 2, pp. 402–417, 2009.
4. Z. Pu, R. Yuan, X. Tan, and J. Yi, “Active robust control of uncertainty and flexibility suppression for air-breathing hypersonic vehicles,” Aerospace Science and Technology, vol. 42, pp. 429–441, 2015.
5. D. Q. Mayne, J. B. Rawlings, C. V. Rao, and P. O. M. Scokaert, “Constrained model predictive control: Stability and optimality,” Automatica, vol. 36, no. 6, pp. 789–814, 2000.
6. W. Tang, W. Long, and H. Gao, “Model predictive control of hypersonic vehicles accommodating constraints,” IET Control Theory & Applications, vol. 11, no. 15, pp. 2599–2606, 2017.
7. X. Tao, N. Li, and S. Li, “Multiple model predictive control for large envelope flight of hypersonic vehicle systems,” Information Sciences, vol. 328, pp. 115–126, 2016.
8. D. O. Sigthorsson, P. Jankovsky, A. Serrani, S. Yurkovich, M. A. Bolender, and D. B. Doman, “Robust linear output feedback control of an airbreathing hypersonic vehicle,” Journal of Guidance, Control, and Dynamics, vol. 31, no. 4, pp. 1052–1066, 2008.

9. X. Tao, J. Yi, Z. Pu, and T. Xiong, "State-estimator-integrated robust adaptive tracking control for flexible air-breathing hypersonic vehicle with noisy measurements," IEEE Transactions on Instrumentation and Measurement, vol. 68, no. 11, pp. 4285–4299, 2019.
10. W. P. M. H. Heemels, K. H. Johansson, and P. Tabuada, "An introduction to event-triggered and self-triggered control," in Proceedings of the 51st IEEE Conference on Decision and Control, Maui, HI, USA, 2012, pp. 3270–3285.
11. X. Ge, Q.-L. Han, X.-M. Zhang, and D. Ding, "Dynamic event-triggered control and estimation: A survey," International Journal of Automation and Computing, vol. 18, no. 6, pp. 857–886, 2021.
12. H. Li and Y. Shi, "Event-triggered robust model predictive control of continuous-time nonlinear systems," Automatica, vol. 50, no. 5, pp. 1507–1513, 2014.
13. K. Hashimoto, S. Adachi, and D. V. Dimarogonas, "Event-triggered intermittent sampling for nonlinear model predictive control," Automatica, vol. 81, pp. 148–155, 2017.
14. J. Zhao and M. Chen, "Dynamic event-triggered robust feedback model predictive tracking control of air-breathing hypersonic vehicle based on disturbance preview," IEEE Transactions on Aerospace and Electronic Systems, vol. 61, no. 2, pp. 3291–3305, 2025.
15. J. Han, "From PID to Active Disturbance Rejection Control," IEEE Transactions on Industrial Electronics, vol. 56, no. 3, pp. 900–906, Mar. 2009.